In-mine (tunnel-to-tunnel) electrical resistance tomography in South African platinum mines

Michael van Schoor[1*] and Andrew Binley[2]

[1] *CSIR, Centre for Mining Innovation, PO Box 395, Pretoria, South Africa*

[2] *Lancaster Environment Centre, Lancaster University, Lancaster, UK*

* *mvschoor@csir.co.za*

Submitted to *Near Surface Geophysics* special issue on "Student-based research"

In-mine (tunnel-to-tunnel) electrical resistance tomography in South African platinum mines

Michael van Schoor and Andrew Binley

ABSTRACT

The applicability of tunnel-to-tunnel electrical resistance tomography (ERT) for imaging disruptive geological structures ahead of mining, in an igneous platinum mining environment is assessed. The geophysical targets of interest are slump structures or 'potholes' that disrupt the lateral continuity of the thin, tabular platinum orebodies of the Bushveld Complex, South Africa. The study involves a combination of model studies, laboratory property measurements and trial surveys. The property studies indicate that the problem reduces to the challenging scenario of a high-resistivity background (orebody horizon) in which an even more resistive target (pothole) is embedded. The model studies show that ERT can potentially image disruptive potholes ahead of mining. It is further demonstrated that the 2D approach can generally be used as a reconnaissance tool, but that a variety of three-dimensional (3D) effects need to be considered, and, in some instances, appropriate corrections should be applied. 3D scenarios that are considered include targets with limited extent perpendicular to the image plane, targets with a relatively small volume and targets that are asymmetrical about the image plane. Other 2D model assumption violations considered include the effect of tunnels and multi-layered backgrounds. Finally, results from an experimental in-mine survey are included to illustrate that ERT can be used to detect and delineate potholes ahead of mining.

Keywords: ERT, tomography, in-mine, tunnel-to-tunnel, 3D effects

INTRODUCTION

The versatility of electrical resistance tomography (ERT) has made it one of the most widely used techniques in near surface geophysics in recent years (Barker and Moore, 1998; Day-Lewis *et al.*, 2005; Ramirez and Daily, 2001; Slater *et al.*, 2000; Zhou and Dahlin, 2003). The strength of ERT lies in the different survey geometry options and the diversity of applications. In this paper, an unconventional and novel application for ERT is considered; that is, the in-mine application (using a tunnel-to-tunnel survey geometry) in deep-level platinum mines of South Africa.

Geological setting

The platinum mineralisation of the Bushveld Complex of South Africa occurs in thin (~1-2 m), tabular orebodies, locally referred to as ‘reefs’. These reefs form part of the Rustenburg Layered Suite (RLS), which is one of the three main stratigraphic units of the complex (Cawthorn, 1999b; The South African Committee for Stratigraphy (SACS), 1980). The mafic and ultramafic rocks of the RLS occur in three arc-shaped areas, which are commonly referred to as the ‘western’, ‘eastern’ and ‘northern’ limbs of the Bushveld Complex (Fig. 1).

The majority of the platinum mining activities occur in the western and eastern limbs and the two primary orebodies are the Merensky Reef and Upper Group 2 chromitite layer (UG2). These, two economic units occur within the Upper Critical Zone, which

consists of alternating layers of pyroxenite, norite, spotted anorthosite, mottled anorthosite and chromitite. The Merensky Reef is defined as the economically exploitable portion of a cyclic unit, which is typically made up of different lithological layers; consequently, the nature of the Merensky Reef may differ from mine to mine, depending on where the mineralisation is concentrated (Leeb-du Toit, 1986; Mossom, 1986; Viljoen *et al.*, 1986a; Viljoen and Hieber, 1986; Viljoen *et al.*, 1986b). However, the Merensky Reef typically contains pyroxenite, melanorite, harzburgite and bronzite. The UG2 is a substantial chromitite layer, usually hosted within a pyroxenite unit. The platinum mineralisation within the Merensky Reef and UG2 are mostly associated with base metal sulphides such as pyrrhotite, pentlandite, chalcopyrite and pyrite (Viljoen and Hieber, 1986).

The platinum orebodies of the Bushveld Complex is of great economic significance as approximately 75% of the world's production and reserves are attributed to it (Cawthorn, 1999a). On a regional scale, the platinum reefs are laterally continuous over vast distances and therefore relatively predictable and easy to mine. On a mine scale, however, the continuity of the platinum reefs is often disrupted by slump structures, known as 'potholes', which may vary in size from a few metres to tens of metres. Potholes can result in either a local distortion or discontinuity in the reef horizon (Fig. 2), which has adverse economic implications. Potholes are often associated with poor ground conditions, which increases support requirements and impacts negatively on safety. The distribution, extent and geometry of potholes are notoriously difficult to predict ahead of mining and the inevitable impact on mining is either a loss of mineable

ground or the need for unplanned and expensive adapted mining practices to negotiate the slumping reef (Van Schoor *et al.*, 2006).

Platinum mines have traditionally relied on borehole logging and aeromagnetic surveys for obtaining structural information prior to developing/extending mines (Düweke and Trickett, 2001). The aeromagnetic technique is used for the mapping of large-scale faults, but is not suitable for mapping mine-scale potholes. No surface geophysical technique is currently used to routinely map these mine-scale features ahead of mining, owing to the relatively small target size, compared to the depth of investigation. One surface technique that has shown some promise, in terms of pothole detection, is 3D reflection seismic technique. This technique has a very high mapping accuracy, which makes it possible to map not only large-scale regional features but also some of the mine-scale potholes. Vertical and horizontal resolutions of approximately 10 m to 15 m and a depth of investigation of several hundred metres can be achieved. Despite the promising capabilities of 3D surface reflection seismics, there is still a need for high-resolution, in-mine geophysical solutions to pothole and IRUP delineation. It must be noted that 3D reflection seismics and high-resolution, in-mine techniques are not competitors – they are applicable to different scales of problems and to different stages of the exploration/mining chain. High-resolution, in-mine techniques are more applicable further down the exploration/mining chain. Most mine-scale potholes have depths of less than approximately 10 m, which rules out routine pothole detection from surface. Furthermore, 3D seismic surveys are relatively expensive and the smaller the survey area, the higher the relative cost. Consequently, a need has arisen for a relatively

inexpensive high-resolution geophysical tool for facilitating short to medium-term planning.

More recently, borehole radar has been used in platinum mines to image potholes ahead of mining (Trickett *et al.*, 2000; Vogt *et al.*, 2005). Borehole radar is used primarily to quantify the geometry or depth of slumping of a known pothole and sub-metre accuracy can be achieved over distances of several hundred metres ahead of mining. However, in order to achieve this, special boreholes need to be drilled ahead of mining. Even if the additional cost of drilling such boreholes is ignored, the successful application of borehole radar does not negate the need for a reconnaissance mapping tool capable of mapping the spatial distribution of potholes ahead of mining in the plane of the near-horizontal orebody.

Adopted methodology

Considering the abovementioned negative impact of potholes, it is not surprising that the platinum mining industry had repeatedly expressed the need for a tactical geophysical tool capable of predicting and delineating pothole occurrences ahead of mining. Research into this problem was initiated at the CSIR's mining research group in 2002. The objective of the associated study summarised here was to assess and benchmark the applicability of in-mine ERT for the routine mapping of reef disruptions ahead of mining, using a two-dimensional (2D) imaging approach and a tunnel-to-tunnel survey geometry (Van Schoor, 2009).

The proposed ERT application differs from more conventional near surface applications in that it does not exploit near surface boreholes or electrodes on the Earth's surface, and the output represents near-horizontal cross-sections rather than vertical sections through the subsurface. In other words, the image plane does not cut across the normal (horizontal) stratification, but is orientated parallel to it (Fig. 3). In a sense, the survey geometry is analogous to that of in-seam seismic tomography or radio imaging, which is sometimes applied in coal mining environments.

The typical depth of underground platinum workings in the Bushveld Complex is a few hundred metres below surface. The ore is accessed and extracted by means of various interconnected excavations or tunnels, i.e., haulages, crosscuts and raises, developed from the main vertical shaft to positions within the reef plane (Fig. 3). It is from these in-reef positions that ore extraction is initiated and the reef is mined out in a systematic, block-by-block fashion. A block is defined as the area between two adjacent raises, and typically has dimensions ranging from 35-200 m (raise spacing) by 100-200 m (raise extent).

In-mine ERT surveys are conducted in a manner similar to that of conventional surface or borehole-based resistivity imaging (Binley and Kemna, 2005; Slater *et al.*, 2000). A typical survey comprises a combination of in-line dipole-dipole measurements along the respective raise tunnels, and tunnel-to-tunnel measurements in which the source and receiver dipoles are located in opposite tunnels. The electrodes are placed along the raise tunnel sidewalls that straddle the unmined survey block. The specific acquisition parameters are usually dictated by the survey site geometry, but a unit electrode spacing

of approximately 1/10th the tunnel spacing is commonly specified. The maximum possible survey site aspect ratio is desired, but a value of between 3:2 and 2:1 is achievable in most cases. A typical in-mine survey would involve between 30 and 50 electrode locations. Galvanic contact with the hard rock sidewalls is typically achieved by inserting expansion bolts into pre-drilled holes filled with electrode coupling gel.

In the quoted study (Van Schoor, 2009), the concept of tunnel-to-tunnel ERT is assessed through a comprehensive model study that covered a wide range of key issues, including the selection of optimum data acquisition, processing and inversion parameters. The model study also investigates the 3D effects on 2D ERT imaging and also explores the option of 3D inversion. The selection of realistic model parameters is aided by a series of laboratory property measurement on core samples from various platinum mines.

A review of previously published research results indicated that the in-mine application of ERT is relatively uncommon. Most previous efforts typically focused on obtaining information from zones close to single tunnels or pilot bores drilled from underground tunnels (Gibert *et al.*, 2006; Jämtlid *et al.*, 1984; Scott *et al.*, 1968; Yaramanci, 2000). There were some reports of cross-hole ERT experiments done form underground tunnels (Noguchi *et al.*, 1991; Ramirez and Daily, 1997a, 1997b), but these surveys were of a small-scale and non-mining nature. Arai (Arai, 1995), and more recently Eso and co-workers (Eso *et al.*, 2006a; Eso *et al.*, 2006b) exploited survey geometries similar to what is considered here; that is, tunnels surrounding an area of interest. These studies, however, essentially represented once-off trial surveys. Sasaki and Matsuo

exploited a tunnel-to-surface geometry for ERT investigations in a copper-scarn mine (Sasaki and Matsuo, 1993), while Kruschwitz and Yaramanci experimented with in-mine ERT in rock salt mines (Kruschwitz and Yaramanci, 2004), but these surveys were limited to looking at fracture characteristics around single excavations.

LABORATORY PROPERTY STUDY

A series of laboratory physical property measurements were conducted on rock samples sourced from a variety of Bushveld Complex platinum mines. These measurements were aimed at providing insight into whether sufficient resistivity contrasts existed between the disruptive geological features (pothole / hangingwall material) and the background rocks (Merensky Reef and UG2). Note that the unique combination of survey geometry and geological problem implies that the geophysical target is in fact represented by the (slumping) host rocks of the environment, while the background rocks in the geophysical model is represented by the tabular orebody and its immediate hanging- and footwall. For the purpose of this paper, only the key results of the property studies are summarised in Table 1. The property measurements comprised a series of electrical resistivity measurements over a range of current injection frequencies. Here we focus on the low frequency values (shown in Table 1), although the reader is referred to Van Schoor (2009) for more details of the spectral response.

MODEL STUDIES

Modelling approach and tools

Owing to the interest in the 3D effects on 2D inversion, the commercial modelling software package *EMIGMA*, from Petros Eikon, Canada was used to generate forward model data sets. *EMIGMA* is a scattering simulation routine, based on the Localized Non-linear (LN) approximation (Groom and Alvarez, 2002; Habashy *et al.*, 1993; Murray, 1997) that enables the 3D modelling of electrical resistivity (and induced

polarisation) responses. The Localized Non-linear approximation is an integral equation solution, in which the integral equation represents the volume of ground with anomalous conductivity; that is, the target anomalies or scatterers. The background conductivity structure is simplified to allow for the associated incident fields to be calculated either analytically or quasi-analytically. The subsurface background structure is represented by a uniform or multi-layered half-space. In physical terms, the integral equation specifies how the anomalous conductivity alters the current flow in the ground from the current distribution that would have flowed (undisturbed) in the background medium. The electric field is calculated at various points inside the target, which is then used as input to the integral equation solution. The resulting output is the current pattern due to the target anomaly. The associated scattered fields can then be derived by integration over the current pattern. The fields are calculated in the frequency domain and are expressed in terms of real and quadrature conductivity components, from which complex resistivity magnitude and phase values can be derived. For the purpose of this paper, only the low frequency magnitude component of the resistivity response is of interest; for more details of modelling of the phase response see van Schoor (2009).

For inversion, the 2D algorithm *CRTomo* (Kemna, 2005a) was used. *CRTomo* is based on the well-known Occam's approach. The inversion scheme utilises a standard Gauss-Newton approach in conjunction with a conjugate gradient (CG) method to solve the numerical problem iteratively. *CRTomo* accounts for resistivity magnitude data noise through two error model parameter inputs: the relative resistance error (*a*) and the absolute resistance error (*b*). The CRTomo inversion algorithm is based on the well-known Tikhonov approach in which an objective function is iteratively minimised. The

iteration process is terminated when an acceptable data misfit target is achieved and the corresponding RMS error approaches one. The target misfit is based on the user defined data error model.

Selected basic model study results

Based on a comprehensive model study (Van Schoor, 2009), not included here, the following modelling parameters were adopted for the tunnel-to-tunnel in-mine ERT application:

- A dipole-dipole-based measurement scheme with multiple dipole lengths; the use of the nearest-neighbour dipole-dipole array supplemented with dipole-dipole measurements for at least one larger dipole length is advocated;
- A conservative noise threshold of 0.1 Ω is assumed throughout the study; this, for example, equates to a reliable voltage threshold of around 2 mV at injected current levels of approximately 20 mA. In the high-resistivity platinum mining environment, the electrode contact resistances are expected to be high and injected current levels may be relatively low, while background noise levels may be relatively high.
- It was demonstrated that, for the typical physical property parameters expected in the Bushveld platinum mines, a maximum tunnel spacing of between 100 m and 200 m was achievable (Fig. 4). It should, however, be noted that for lower than expected background resistivities, the recorded voltages are also lower, which may result in a reduced number of measurements and an associated deterioration in imaging performance.

One of the principal aims of the modelling study is to examine the viability of using a 2D imaging method for studying an inherently 3D problem. Fig. 5 shows a generic 3D in-mine model in which T1 and T2 represent the two coplanar lines of electrodes located along the sidewalls of two tunnels. The pothole target is simulated by a relatively small localised target body with a total extent *h* in the third (vertical) dimension. For relatively large values of *h*, compared to the tunnel spacing, the 3D model response should approach that of the equivalent 2D model. The default background and target resistivity properties used were as follows: 10 000 Ωm for the (partly mineralised) background; and 50 000 Ωm for the (pothole) targets. A series of model studies were conducted in which the objective was to assess the applicability of 2D ERT in an environment where the simplifying assumptions of 2D inversion are expected to be violated. The key results of these model studies are summarised below.

In the first batch of simulations**,** the generic 3D model was perturbed in terms of the target's vertical extent and its symmetry with respect to the image plane. Selected results are shown in Fig. 6 and Fig. 7. These simulations were extended to consider a wider range of variables for the purpose of more comprehensive benchmarking. For example, the target size and location within the (2D) image plane as well as the background:target property contrast were also varied. Selected results appear in Fig. 8.

The results show that the 2D inversion approach manages to reconstruct the target reasonably well in most cases, provided the vertical extent of the localised target is such that it can be approximated by a 2D body. When the target is small compared to the

tunnel spacing, or when it does not have significant extent above and below the image plane, the 2D target assumption breaks down and the imaging performance is compromised. In such cases the target resolution decreases slightly and the recovered image contrast approaches levels that would not be detectable in practice. Fig. 8 also illustrates how the location of the target within the 2D image plane plays a key role in imaging performance. Targets that lie in zones of low sensitivity (central zone between lines of electrodes) are more difficult to detect and resolve than targets that are located in zones of high sensitivity, close to the lines of electrodes. Some targets that violate the 2D target assumption, such as small targets or those that are asymmetrical with respect to the image plane may only be detectable if they are located in zones of high sensitivity.

Tunnel effect and corrections

Up to now the simplifying assumption of a geoelectrical full space has been applied. The effect of tunnels and mining cavities is, however, not expected to be negligible in all cases and, consequently, the significance of the tunnel effect was assessed through modelling. For example, Fig. 9 depicts a typical 3D scenario to be expected in the platinum mines; that is, two adjacent, co-planar raise tunnels. These tunnels are typically 1.5 m wide and 2 m high. Simulations were conducted to assess the manifestation of the tunnel effect (both with and without a pothole target) on tomographic output images. Fig. 10 shows a series of associated results.

The first output image in Fig. 10 shows how prominently the tunnel response may manifest on an ERT output image in the absence of a pothole target. The second image

shows that even if a target is present, the tunnel effect is still evident and the image is contaminated by unwanted artefacts. The last two images shows two approaches to dealing with the tunnel effect: Firstly one could simply discard, prior to inversion, those data points that are most significantly affected by the tunnel response. A better approach is, however, to apply a correction for the tunnels, based on the known geometry of the tunnels. One possible approach is to apply an approximate correction to the response of the full model (R_{MODEL}), which includes the tunnels, prior to inversion by subtracting the calculated tunnel effect from the full-model transfer resistances. In other words, instead of inverting R_{MODEL}, the reduced data set ($R_{REDUCED}$) is inverted; that is:

$$R_{REDUCED} = R_{MODEL} - R_{TUNNELS} \quad (1)$$

The effect of layering

A further 3D effect that was considered in the 2D vs. 3D model study was the violation of the 2D background assumption; in other words, the effect of layering above and/or below the 2D image plane. This type of scenario would become relevant where the thin tabular reef has a significant property contrast with the immediate hanging- and footwall and/or where a thin contrasting layer is, for example, present in the immediate hangingwall. Fig. 11 depicts two such scenarios. In the first case the image plane occurs within a thin, relatively conductive reef layer. The second model constitutes a more complex scenario – a multi-layered earth in which the hangingwall layers slump down to disrupt the continuity of the reef and immediate hangingwall layers. In both cases the standard magnitude inversion results do reflect the target anomaly, but the output image is characterised by some degree of target distortion and contamination by unwanted

artefacts (Fig. 12). This inferior inversion performance is the result of the 2D inversion algorithm attempting to fit a uniform background to the data which includes the response of a non-uniform background. As in the case of the tunnel-effect, the inversion performance can be improved drastically by applying a correction based on *a priori* geological and mining information (Fig. 12).

It should be noted that 3D inversion, when applied appropriately, could be used as an alternative approach to address inversion problems that cannot be handled correctly by more conventional 2D algorithms. For example, in a thin-reef layer scenario, a standard 2D inversion may fail at reconstructing a subtle resistivity target located within the thin layer / image plane. In the 3D approach the inversion may be guided by specifying a starting model and reference model which is based on the known thin reef layered earth model (without the target). The idea behind guiding the inversion in this way is to attempt to produce an output model that emulates the thin reef (reference) model and, in doing so, emphasises the differences between the latter and the true model structure (which is assumed to be unknown). The 3D approach is arguably the recommended approach for future in-mine surveys. However, it should be emphasised that the decision to assess the applicability of 2D rather than 3D imaging in this study was based on the very specific needs of the mining industry. Owing to the production-driven pressures of deep level platinum mining, fast turnaround times and ease of use are key requirements of any in-mine geophysical applications. The 2D (coplanar or in-reef) data-acquisition and imaging strategy described here is already pushing the limits in terms of the above criteria and, consequently, true 3D data acquisition involving additional electrode locations at positions away from the reef plane and even 3D

inversion based on 2D data sets, is, at this stage, considered as not viable. Mines would much rather embrace the concept of fast, and relatively user-friendly, reconnaissance-style 2D tomographic surveys than the more complicated 3D approach surveys. Suspected pothole anomalies could then either be followed up with more detailed tomographic surveys or with another high-resolution geophysical technique such as borehole radar.

CASE STUDY – WATERVAL PLATINUM MINE

Site description

In May 2009, an ERT trial survey was conducted at Anglo Platinum's Waterval Mine near Rustenburg. Waterval Mine is a bord-and-pillar, mechanised operation where the UG2 is being mined. The stoping width (mining height) at Waterval is approximately 1.8 m and includes the UG2 and a portion of the pegmatoidal pyroxenite of the immediate footwall, which is also slightly mineralised. Two other significant chromitite bands occur in the hangingwall: a 20 cm chromitite seam, the Leader Seam, occurs approximately 1.4 m above the UG2, and the Chromitite Triplets, with a combined thickness of approximately 30 cm, occur a further 3.5-4 m higher up in the succession. The immediate hangingwall of the UG2 consists mainly of feldspathic pyroxenite with some norite/melanorite. The chosen test site is located approximately 450 m below surface in an area where a relatively large pothole, with a diameter of approximately 50 m, was encountered. The bulk of the affected area was left unmined as a large natural support pillar (Fig. 13). The primary objective of the survey was thus to determine

whether ERT could discriminate between the abovementioned portion of UG2 reef and the surrounding pothole.

The original plan involved using the two long sides of the pillar for cross-line tunnel-to-tunnel measurements. However, shortly before the survey it became evident that, due to installed ventilation barriers along the southern edge of the pillar (see Fig. 13), access to the developments south of this line was not possible. In the original survey plan, a total of 41 electrodes, using a unit electrode spacing of 3 m, would have been deployed along the northern, western and southern sides of the pillar; as a result of the ventilation barrier, only 15 electrodes along the northern pillar face and 11 electrodes along the western side, could ultimately be deployed. The survey was thus reduced to a 26-electrode configuration that crosses the inferred boundary between the pothole and the unaffected reef.

Data acquisition

Resistivity data was acquired using a Zonge GDP-32^{II} system. A ‘skip 0’ dipole-dipole measurement scheme (Slater *et al.*, 2000) was employed between electrodes 1 and 26 and this was supplemented with some ‘skip 1’ measurements between electrodes 1 and 15. ‘Skip 0’ refers to a basic nearest-neighbour dipole-dipole measurement scheme in which the dipole length and incremental increase in dipole spacing are equal to the unit electrode spacing. For the ‘skip 1’ scheme, the dipole length and incremental increase in dipole spacing are equal to double the unit electrode spacing.

Time constraints prevented further measurements. For the purpose of noise analysis, normal and reciprocal measurements were acquired for the majority of the ‘skip 0’

measurements. The resulting data set comprised a relatively small number of 159 data points. In contrast the envisaged cross-line survey configuration (utilising the two long sides of the survey area and assuming no time constraints) would have comprised 30 electrodes and approximately 350 ‘skip 0’ and 250 ‘skip 1’ measurements. The data were acquired at a base frequency of 0.125 Hz; coupling with the rock was achieved through 10 mm x 100 mm sleeve anchor bolts inserted into pre-drilled holes filled with electrode coupling gel. Current injection levels were generally in the order of 50 mA at an applied voltage of 300-400 V.

Field data quality appeared to be good, based on in-field measurement repeatability checks and observed standard data errors. However, post-survey analysis of the reciprocal measurements suggested relatively high systematic errors, with the relative transfer resistance error between approximately 12% and 15%. The high in-mine noise levels may be attributed to the presence of electrically powered machinery operating in nearby underground developments and as part of the mine’s hoisting infrastructure.

Simulation and field result

As part of the analysis, a simulation study was performed prior to inverting the field data. The simplified model shown in Fig. 14a simulates the actual pothole scenario and the measurement scheme that was used. In the model, the UG2 was assigned a resistivity of 3000 Ωm and a property contrast of 5:1 with the surrounding (hangingwall) material was assumed; that is, a background resistivity of 15 000 Ωm. The survey area was discretised into 1 m x 1 m cells for the purpose of employing the

finite element based *CRMod* and *CRTomo* modelling and inversion software (Kemna, 2005b, 2005a). The modelling results, shown in Fig. 14b and Fig. 14c reveal how the limited coverage resulting from the sub-optimum electrode configuration produces a somewhat distorted target anomaly – the UG2 anomaly is biased towards the electrodes on the western side of the pillar and is not resolved on the southern side of the ventilation barrier. The associated normalised accumulated sensitivity maps (Binley and Kemna, 2005), shown in Fig. 14d and Fig. 14e, respectively, further highlight the decreased sensitivity resulting from using the reduced number of electrodes.

The image of the inverted, tunnel-corrected field data is shown in Fig. 15. The image presented here was based on a data set of approximately 110 data points for which a relative magnitude error level of 14.5% was assumed. It should also be noted that the difference between the tunnel-corrected and uncorrected output images was found to be negligible and this may be attributed to the dominant manifestation of the target features described below. The output image reveals two distinct anomalous conductive zones in a relatively resistive background:

- The portion of unaffected UG2 reef in the SW corner of the survey area manifests clearly on the output image. As anticipated, and predicted by the model study, the transition between UG2 and pothole is easily detected, but the mapping accuracy of the edge is affected by the electrode coverage / sensitivity issues highlighted earlier.
- The conductive patches located along the stretch between electrodes 1 and 10 was at first thought to be noise artefacts, but following post-survey discussions with the

mine geologist, a feasible explanation for these anomalies became evident: It is estimated that this particular pothole, despite its large diameter, has a relatively shallow slump/depth of approximately 4-5 m, which is approximately equivalent to the distance between the Chromitite Triplets and the UG2 (Pers. Comm., R. Makgato, June 2009). Also, the other significant chromitite seam, the Leader Seam, occurs between the UG2 and the Chromitite Triplets. It is thought that, as one moves from the edge of the pothole towards the central part of the pothole, these relatively conductive chromitite horizons slump down to the normal UG2 and development level and, consequently, also approach or even intersect the image plane. This proximity/intersection manifests as the observed patches of increased conductivity between electrodes 1-10.

CONCLUSION

Through a combination of physical property analyses and model studies it has been established that 2D ERT can be used as reconnaissance tool for detecting platinum reef disruptions ahead of mining. Other geophysical imaging techniques such as the aeromagnetic, borehole radar and 3D reflection seismic techniques do not provide the same in-reef pothole delineation capabilityoffered by in-mine ERT – the advantage of the ERT approach is primarily due to the tunnel-to-tunnel survey geometry by which the area of interest can effectively be ‘framed’.

The model study also highlighted the fact that 3D effects cannot be ignored in mine surveys. Where possible, *a priori* geological and mining information should be used to

apply appropriate corrections or to better constrain the 2D inversion, thereby minimizing the impact of unwanted 3D effects. However, with technological advances made in recent years, in terms computing power and 3D inversion algorithms, the use of full 3D inversion in future in-mine tomographic surveys has become a realistic option. Alternatively, better constrained 2D inversion approaches could be considered. Further work is also recommended to determine whether meaningful IP measurements can be acquired on a routine basis in underground mining environments and whether the IP technique would be able to add value in terms of discriminating between potholes and other reef disruption targets.

The findings of this study may also have wider application, beyond mining geophysics. The imaging applications considered here are analogous to the typical cross-borehole ERT scenario and many of the findings may therefore have relevance to other applications and disciplines where ERT is applied, such as in hydrogeological studies. Furthermore, the somewhat unconventional geometry considered in the mining case; that is, imaging in the plane of a horizontal layer, may also be applied to geometrically similar near-surface problems. For example, in civil engineering ERT could be used to image the integrity of concrete slabs in cases where access for geophysical monitoring is only available around the sides of the (horizontal) slab. The imaging of anomalous features within earth layers immediately below infrastructure such as buildings or dams is another possible analogous application. Even within mining, the application is not necessarily restricted to platinum mining. Many ore deposits of different commodities also occur as near-horizontal, tabular deposits and are mined using conventional mining

493 layouts as is described in this paper. The in-mine application of ERT might thus be a
494 viable option in other second-phase mineral exploration environments.
495
496 **ACKNOWLEDGEMENTS**
497 We would like to acknowledge the CSIR for sponsoring and supporting the research.
498 The participants of the PlatMine Research Collaborative Programme are thanked for
499 funding and supporting parts of the study. Individual platinum mining houses and mines
500 are acknowledged for permission to publish mine specific data and information.
501

REFERENCES

Arai, E. 1995. A resistivity tomography test survey in the Toyoha mine, Hokkaido, Japan. Exploration Geophysics, 25, 45-50.

Barker, R. D. & Moore, J. 1998. The application of time-lapse electrical tomography in groundwater studies. Leading Edge, 17(10), 1454-1458.

Binley, A. & Kemna, A. 2005. DC resistivity and induced polarisation methods. In Y. Rubin & S. S. Hubbard (Eds.), Hydrogeophysics: 129-156. New York: Springer.

Cawthorn, R. G. 1999a. Platinum in South Africa. South African Journal of Science, 95, 481-489.

Cawthorn, R. G. 1999b. The discovery of the platiniferous Merensky Reef in 1924. South African Journal of Geology, 102(3), 178-183.

Day-Lewis, F., Singha, K., & Binley, A. 2005. Applying petrophysical models to radar travel time and electrical resistivity tomograms: Resolution-dependent limitations. Journal of Geophysical Research, 110(B08206).

Düweke, W. & Trickett, J. C. 2001. Three-dimensional reflection seismics as a tool to optimise mine design, planning and development in the Bushveld Igneous Complex. Paper presented at the 7th Biennial SAGA Conference and Exhibition, Drakensburg, South Africa.

Eso, R. A., Maxwell, M., Oldenburg, D. W., & Unrau, J. 2006a. Delineation of water inflow in an underground potash mine with 3-D electrical resistivity imaging. Paper presented at the SAGEEP.

Eso, R. A., Oldenburg, D. W., & Maxwell, M. 2006b. Application of 3D electrical resistivity imaging in an underground potash mine. Paper presented at the Society of Exploration Geophysicists (SEG) Annual Conference, New Orleans.

Gibert, D., Nicollin, F., Kergosien, B., Bossart, P., Nussbaum, C., Grislin-Mouëzy, A., Conil, F., & Hoteit, N. 2006. Electrical tomography monitoring of the excavation damaged zone of the Gallery 04 in the Mont Terri rock laboratory: Field experiments, modelling, and relationship with structural geology. Applied Clay Science, 33, 21-34.

Groom, R. W. & Alvarez, C. 2002. 3D EM Modelling - Application of the Localised non-linear approximator to near surface applications. Paper presented at the SAGEEP.

Habashy, T. M., Groom, R. W., & Spies, B. R. 1993. Beyond the Born and Rytov Approximations: A Nonlinear Approach to Electromagnetic Scattering. Journal of Geophysical Research, 98, 1759-1775.

Jämtlid, A., Magnusson, K., Olsson, O., & Stenberg, L. 1984. Electrical borehole measurements for the mapping of fractures zones in crystalline rock. Geoexploration, 22, 203-216.

Kemna, A. 2005a. CRTomo - 2D Complex Resistivity Inversion.

Kemna, A. 2005b. CRMod, 2.5D Geoelectrical Modelling Tool, Version 1.2ip ed.

Kruschwitz, S. & Yaramanci, U. 2004. Detection and characterisation of the disturbed rock zone in claystone with the complex resistivity method. Journal of Applied Geophysics, 57, 63-79.

Leeb-du Toit, A. 1986. The Impala Platinum Mines. In C. R. Anhaeusser & S. Maske (Eds.), Mineral Deposits of Southern Africa, Vol. II: 1091-1106. Johannesburg: Geological Society of South Africa.

Mossom, R. J. 1986. The Atok Platinum Mine. In C. R. Anhaeusser & S. Maske (Eds.), Mineral Deposits of South Africa, Vol. II: 1143-1154. Johannesburg: Geological Society of South Africa.

Murray, I. R. 1997. On extending the localized non-linear approximation to inductive modes. Paper presented at the 59th EAGE Conference, Geneva, Switzerland.

Noguchi, K., Goto, S., Yuda, T., Furaya, K., Shibamoto, M., & Nishino, H. 1991. In-situ experimental study on resisitivity tomography in tunnels. Paper presented at the 7th ISRM International Congress on Rock Mechanics, Aachen.

Ramirez, A. & Daily, W. 1997a. Electrical resistivity monitoring of the drift scale test in Yucca Mountain. Livermore, CA: Lawrence Livermore National Laboratory.

Ramirez, A. & Daily, W. 1997b. Electrical resistivity monitoring of the single heater test in Yucca Mountain. Livermore, CA: Lawrence Livermore National Laboratory.

Ramirez, A. & Daily, W. 2001. Electrical imaging at the large block test - Yucca mountain, Nevada. Journal of Applied Geophysics, 46, 85-100.

Sasaki, Y. & Matsuo, K. 1993. Surface-to-Tunnel Resistivity Tomography at the Kamaishi Mine. Batsuri-Tansa, 46(2), 128-133.

Scott, J., Lee, F., Carroll, R., & Robinson, C. 1968. The relationship of geophysical measurements to engineering and construction parameters in the Straight Creek Tunnel pilot bore, Colorado. International Journal of Rock Mechanics and Mining Science and Geomechanics Abstracts, 5, 1-30.

Slater, L., Binley, A., Daily, W., & Johnson, R. 2000. Cross-hole electrical imaging of a controlled saline tracer injection. Journal of Applied Geophysics, 44, 85-102.

The South African Committee for Stratigraphy (SACS). 1980. *Stratigraphy of South Africa, Handbook 8, Part 1: Lithostratigraphy of the Republic of South Africa, South West*

Africa/Namibia and the Republics of Bophuthatswana, Transkei and Venda. Pretoria: Department of Mineral and Energy Affairs, Geological Survey.

Trickett, J. C., Stevenson, F., Vogt, D., Mason, I., Hargreaves, J., Eybers, H., Fynn, R., & Meyering, M. 2000. The application of borehole radar to South Africa's ultra-deep gold mining environment. Paper presented at the Eighth International Conference on Ground Penetrating Radar.

Van Schoor, M., Du Pisani, P., & Vogt, D. 2006. High-resolution, short-range, in-mine geophysical techniques for the delineation of South African orebodies. South African Journal of Science, 102, 355-360.

Van Schoor, M. 2009. *Using electrical resistance tomography (ERT) and induced polarisation (IP) tomography to map potholes and iron-rich ultramafic pegmatite bodies in South African platinum mines*. PhD thesis, Lancaster University.

Viljoen, M. J., de Klerk, W. J., Coetzer, P. M., Hatch, N. P., Kinloch, E., & Peyerl, W. 1986a. The Union Section of Rustenburg Platinum Mines Limited with reference to the Merensky Reef. In C. R. Anhaeusser & S. Maske (Eds.), Mineral Deposits of Southern Africa, Vol. II: 1061-1090. Johannesburg: Geological Society of South Africa.

Viljoen, M. J. & Hieber, R. W. 1986. The Rustenburg Section of Rustenburg Platinum Mines Limited, with reference to the Merensky Reef. In C. R. Anhaeusser & S. Maske (Eds.), Mineral Deposits of Southern Africa, Vol. II: 1107-1134. Johannesburg: Geological Society of South Africa.

Viljoen, M. J., Theron, J., Underwood, B. M., Walters, J., Weaver, J., & Peyerl, W. 1986b. The Amandelbult Section of Rustenburg Platinum Mines Limited with reference to the Merensky Reef. In C. R. Anhaeusser & S. Maske (Eds.), Mineral Deposits of Southern Africa, Vol. II: 1041-1060. Johannesburg: Geological Society of South Africa.

Vogt, D., Van Schoor, M., & Du Pisani, P. 2005. The application of radar techniques for in-mine feature mapping in the Bushveld Complex of South Africa. The Journal of the South African Institute of Mining and Metallurgy, 105, 447-452.

Yaramanci, U. 2000. Geoelectric exploration and monitoring in rock salt for the safety assessment of underground waste disposal sites. Journal of Applied Geophysics, 44, 181-196.

Zhou, B. & Dahlin, T. 2003. Properties and effects of measurement errors on 2D resistivity imaging surveying. Near Surface Geophysics, 1(3), 105-117.

LIST OF TABLES

TABLE 1

Summary of physical properties for main categories of platinum rocks.

LIST OF FIGURES

FIGURE 1

Locality map showing the Rustenburg Layered Suite of the Bushveld Complex.

FIGURE 2

Simplified schematic of typical potholes scenarios. Here, the reef layer is transgressed by one or more slumping hangingwall layers; the reef is either pinched out in the pothole or follows the topography of the pothole.

FIGURE 3

Schematic of a conventional platinum mining layout. The yellow shaded plane represents the reef horizon, which is accessed through the series of tunnels shown. The to-be-mined area between adjacent raise tunnels (shaded in blue) also represents the area to be imaged.

FIGURE 4

Selected ERT range model study results. The caption above each figure shows the number of data points remaining (out of a total of 1375) following the application of a 0.1 Ω noise threshold. The colour bar shows $\log_{10}$ resistivity (in Ωm).

FIGURE 5

Generic 3D model used in the model studies. T1 and T2 represent the two coplanar lines of electrodes that would, in practice, be located along the sidewalls of two tunnels.

FIGURE 6

Inversion results showing effect of decreasing 3D extent of target; h_A and $_{hB}$ represent the target extent above and below the image plane. Background resistivity is 10 000 Ωm and target resistivity is 50 000 Ωm. A 2% relative magnitude error was added to the data prior to inversion. In the inversion error model the following parameters were used: a = 2.0%, b = 0.001 mΩ. Images are displayed using the full recovered image range (shown below each image). The colour bar shows $\log_{10}$ resistivity (in Ωm).

FIGURE 7

Inversion results for 3D targets that are not symmetrical with respect to the image plane; h_A and h_B represent the target extent above and below the image plane*;* h_{TOP} represents the top level of a target that lies below the image plane. Background resistivity is 10 000 Ωm and target resistivity is 50 000 Ωm. A 2% relative magnitude error was added to the data prior to inversion. In the inversion error model the following parameters were used: a = 2.0%, b = 0.001 mΩ. Images are displayed using the full recovered image range (shown below each image). The colour bar shows $\log_{10}$ resistivity (in Ωm).

FIGURE 8

ERT inversion results showing the effect of varying target location and target size. The colour bar shows $\log_{10}$ resistivity (in Ωm).

FIGURE 9

3D model used to simulate a tunnel-to-tunnel scenario.

FIGURE 10

Correcting for tunnel – induced artefacts in the inversion. The colour bar shows $\log_{10}$ resistivity (in Ωm).

FIGURE 11

Thin reef model with centrally located 3D target (left) and a model used to investigate the effect of multiple layers and a slumping reef (right). In both cases the two tunnels, T1 and T2, are spaced 30 m apart. The green dashed lines in the second model indicate the effect of the assumed pothole on the respective layer boundaries; the hangingwall layers slump downward by approximately 6 m, the reef is not pinched out due to the slumping but only thins out – the slumping portion effectively forms a 'bowl' in 3D space with the inside filled with (immediate) hangingwall material. The olive-coloured block represents the block model equivalent of the slump structure or target – effectively a 6 m portion of the upper hangingwall layers cutting across the reef and immediate hangingwall layer. The two tunnels, T1 and T2, are spaced 30 m apart.

FIGURE 12

Inversion results for the 3D models depicted in Figure 10. In each case the first image represents the uncorrected results, while the second image shows the result following a difference-based correction applied to account for the interfering effect of layering in the background.

FIGURE 13

Schematic of ERT survey area at Waterval Mine. The darker shaded south-western corner of the large pillar represents a zone of UG2 reef that is not affected by the pothole, while the rest of the pillar effectively lies within the pothole structure. The orange dotted line indicates where the UG2 reef starts slumping, while the green dotted line indicates where the reef slumps into the footwall, below the floor of the developments.

FIGURE 14

Waterval Mine ERT simulation model (a) and modelling results (b and c). Normalised accumulated sensitivity maps for the scenarios in (b) and (c) are shown in (d) and (e), respectively. These simulations highlight the difference in imaging performance when exploiting a total of 41 electrodes as was originally planned versus using only 26 electrodes as in the actual mine survey

FIGURE 15

Waterval Mine ERT field data inversion result.

TABLES AND FIGURES

TABLE 1
Summary of physical properties for main categories of platinum rocks.

	Resistivity range (Ωm)
Merensky and UG2 Reef (geophysical background)	10^3-10^4
Host rock (pothole) material (geophysical target)	10^4-10^5
Expected resistivity contrast pothole:reef	3:1 to 7:1
Expected phase contrast Reef:pothole	3:1 to 7:1

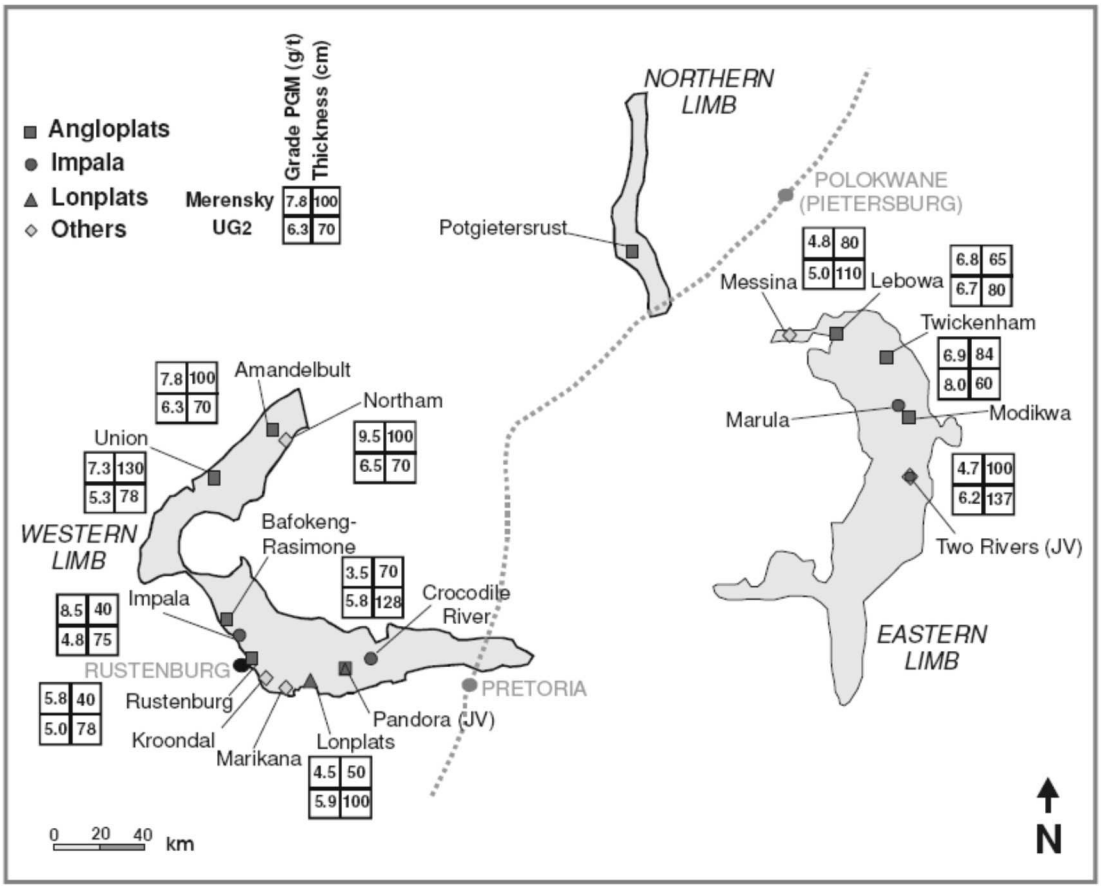

FIGURE 1
Locality map showing the Rustenburg Layered Suite of the Bushveld Complex.

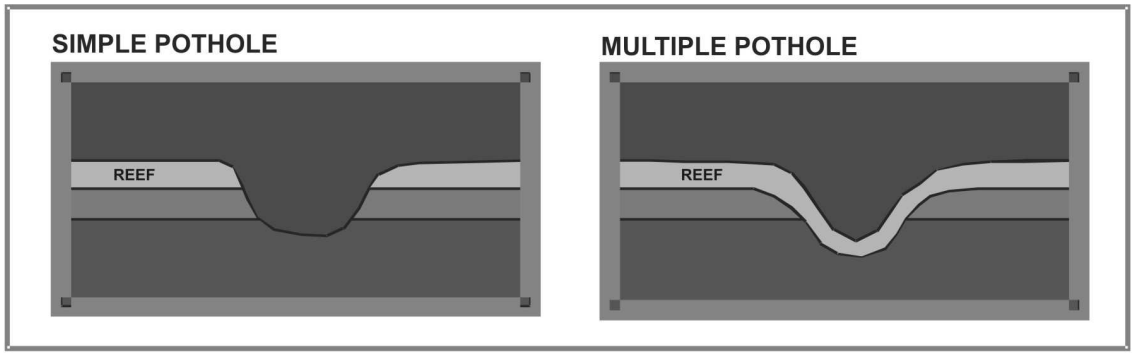

FIGURE 2
Simplified schematic of typical potholes scenarios. Here, the reef layer is transgressed by one or more slumping hangingwall layers; the reef is either pinched out in the pothole or follows the topography of the pothole.

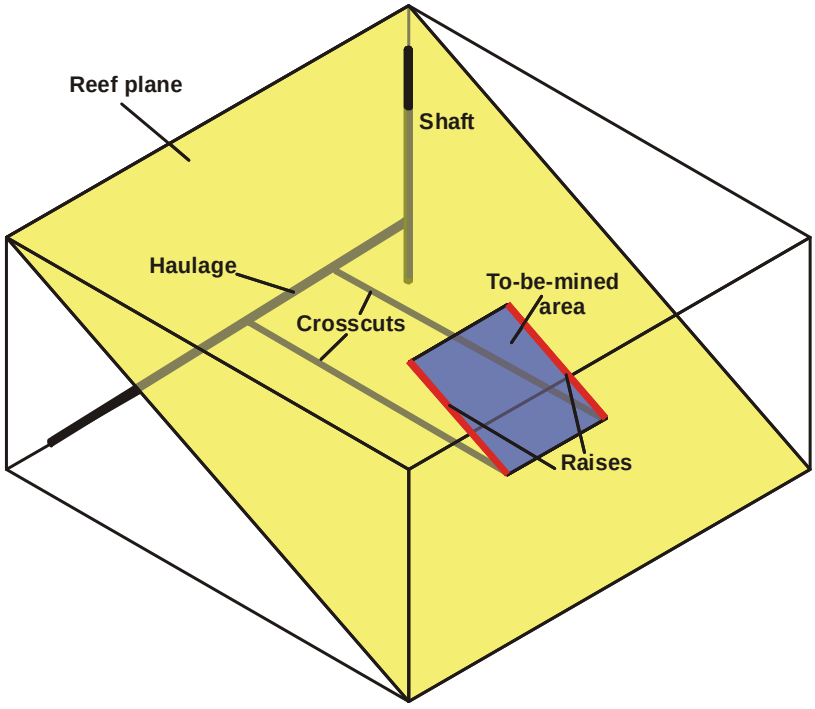

FIGURE 3
Schematic of a conventional platinum mining layout. The yellow shaded plane represents the reef horizon, which is accessed through the series of tunnels shown. The to-be-mined area between adjacent raise tunnels (shaded in blue) also represents the area to be imaged.

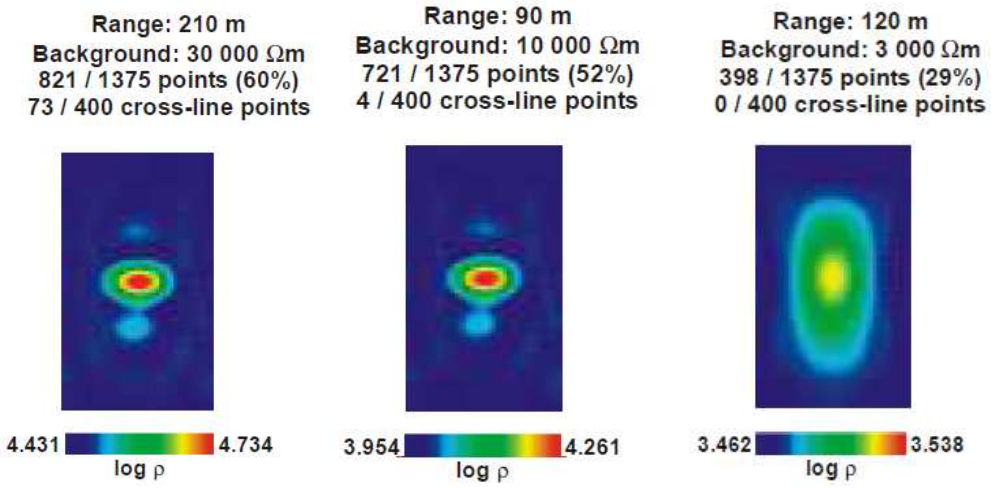

FIGURE 4
Selected ERT range model study results. The caption above each figure shows the number of data points remaining (out of a total of 1375) following the application of a 0.1 Ω noise threshold. The colour bar shows $\log_{10}$ resistivity (in Ωm).

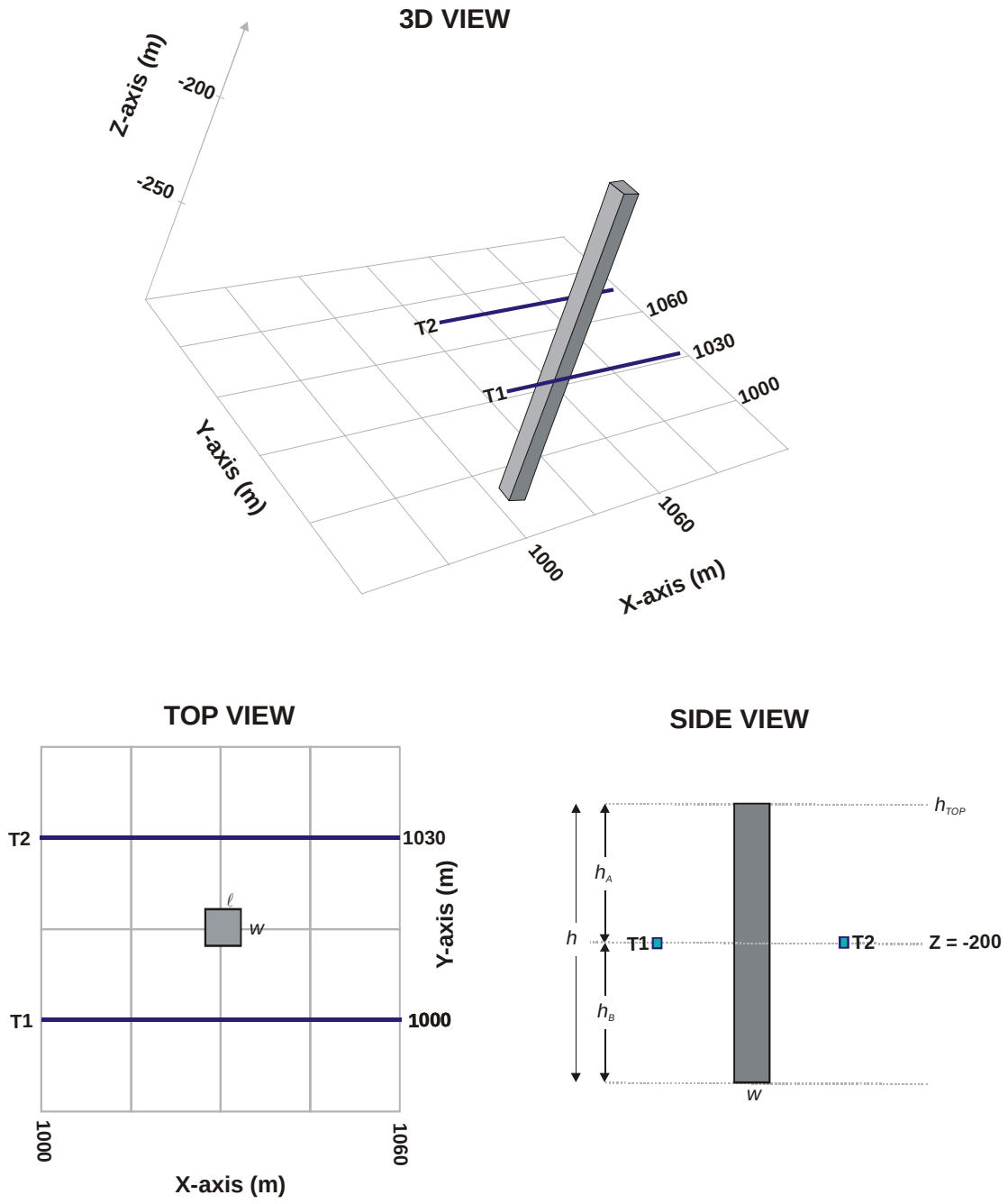

FIGURE 5
Generic 3D model used in the model studies. T1 and T2 represent the two coplanar lines of electrodes that would, in practice, be located along the sidewalls of two tunnels.

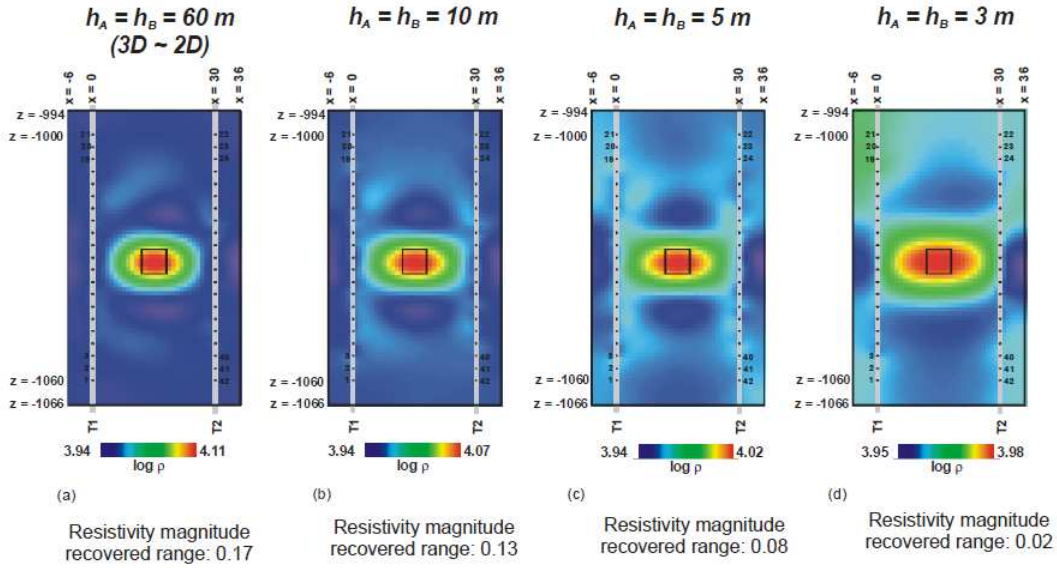

FIGURE 6

Inversion results showing effect of decreasing 3D extent of target; h_A and $_{hB}$ represent the target extent above and below the image plane. Background resistivity is 10 000 Ωm and target resistivity is 50 000 Ωm. A 2% relative magnitude error was added to the data prior to inversion. In the inversion error model the following parameters were used: a = 2.0%, b = 0.001 mΩ. Images are displayed using the full recovered image range (shown below each image). The colour bar shows $\log_{10}$ resistivity (in Ωm).

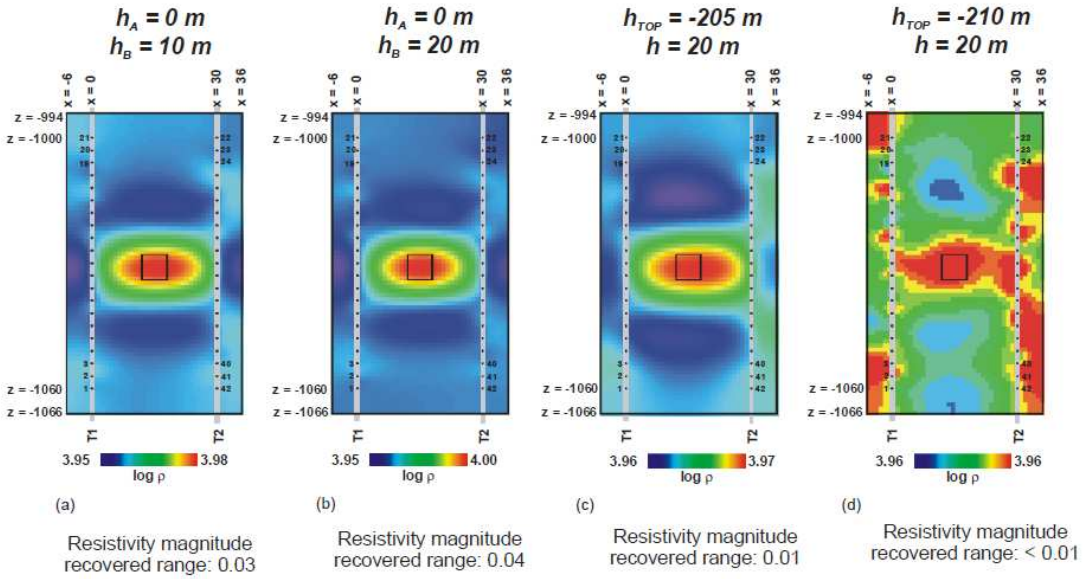

FIGURE 7
Inversion results for 3D targets that are not symmetrical with respect to the image plane; h_A and h_B represent the target extent above and below the image plane; h_{TOP} represents the top level of a target that lies below the image plane. Background resistivity is 10 000 Ωm and target resistivity is 50 000 Ωm. A 2% relative magnitude error was added to the data prior to inversion. In the inversion error model the following parameters were used: a = 2.0%, b = 0.001 mΩ. Images are displayed using the full recovered image range (shown below each image). The colour bar shows $\log_{10}$ resistivity (in Ωm).

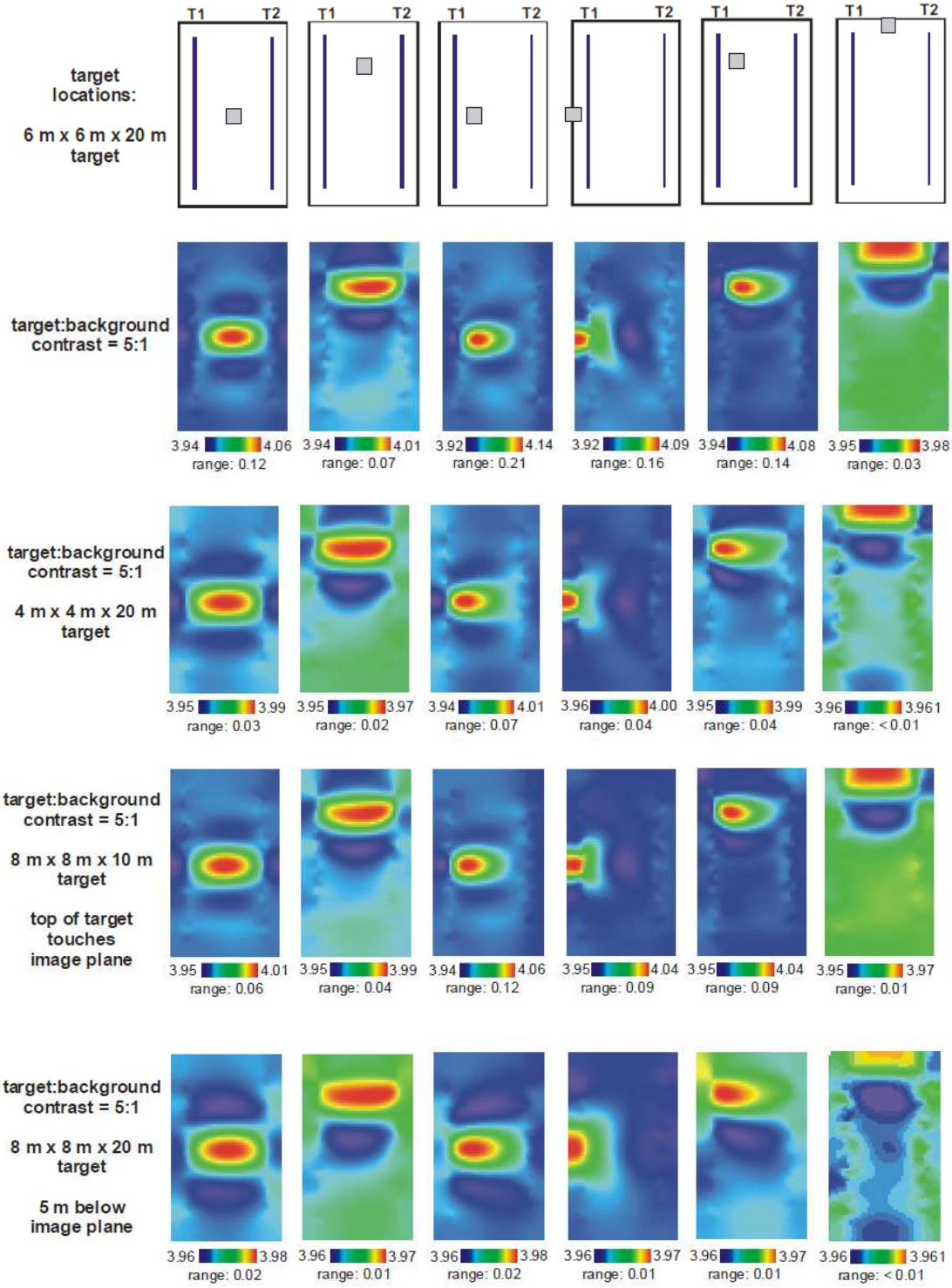

FIGURE 8
ERT inversion results showing the effect of varying target location and target size. The colour bar shows $\log_{10}$ resistivity (in Ωm).

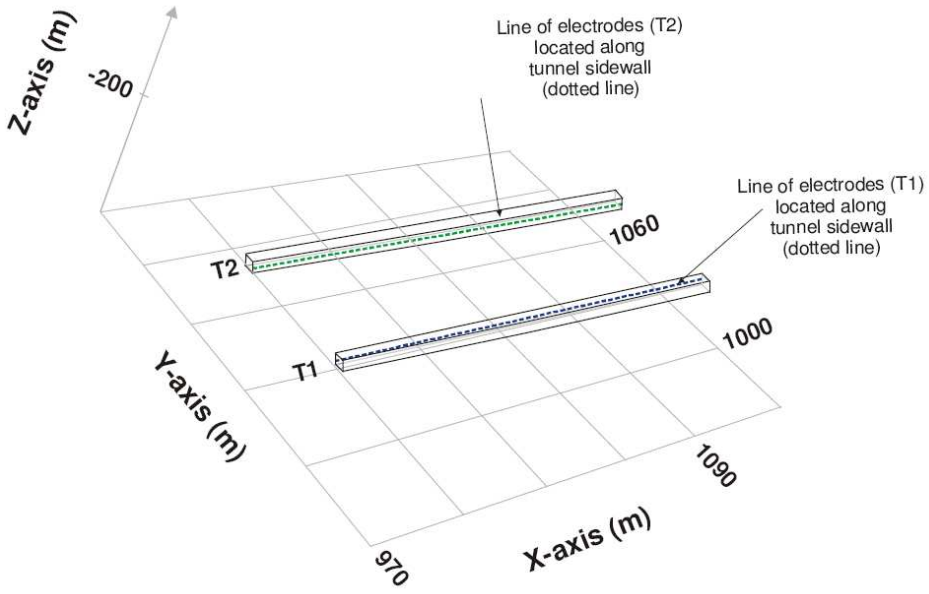

FIGURE 9
3D model used to simulate a tunnel-to-tunnel scenario.

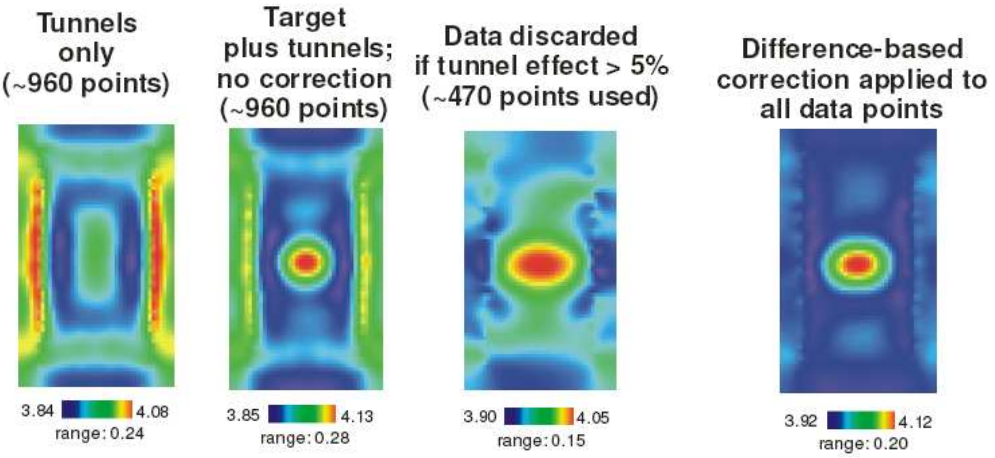

FIGURE 10
Correcting for tunnel – induced artefacts in the inversion. The colour bar shows $\log_{10}$ resistivity (in Ωm).

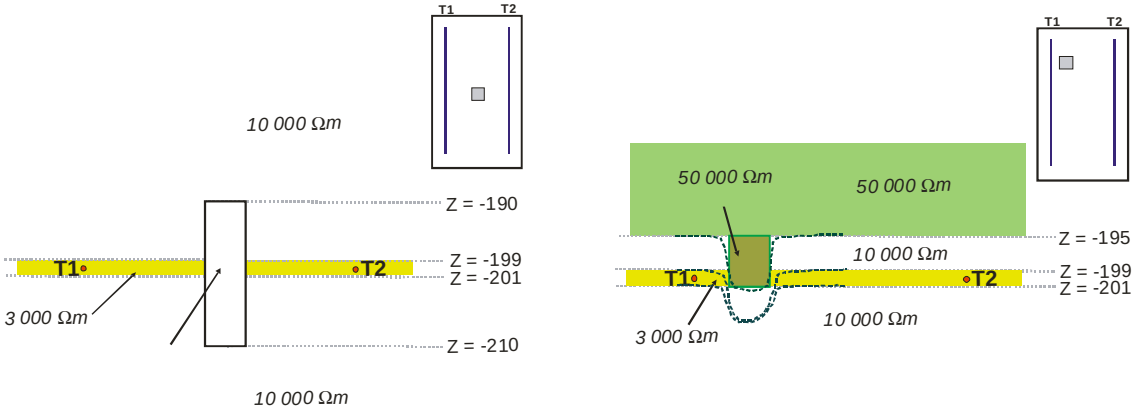

FIGURE 11
Thin reef model with centrally located 3D target (left) and a model used to investigate the effect of multiple layers and a slumping reef (right). In both cases the two tunnels, T1 and T2, are spaced 30 m apart. The green dashed lines in the second model indicate the effect of the assumed pothole on the respective layer boundaries; the hangingwall layers slump downward by approximately 6 m, the reef is not pinched out due to the slumping but only thins out – the slumping portion effectively forms a 'bowl' in 3D space with the inside filled with (immediate) hangingwall material. The olive-coloured block represents the block model equivalent of the slump structure or target – effectively a 6 m portion of the upper hangingwall layers cutting across the reef and immediate hangingwall layer. The two tunnels, T1 and T2, are spaced 30 m apart.

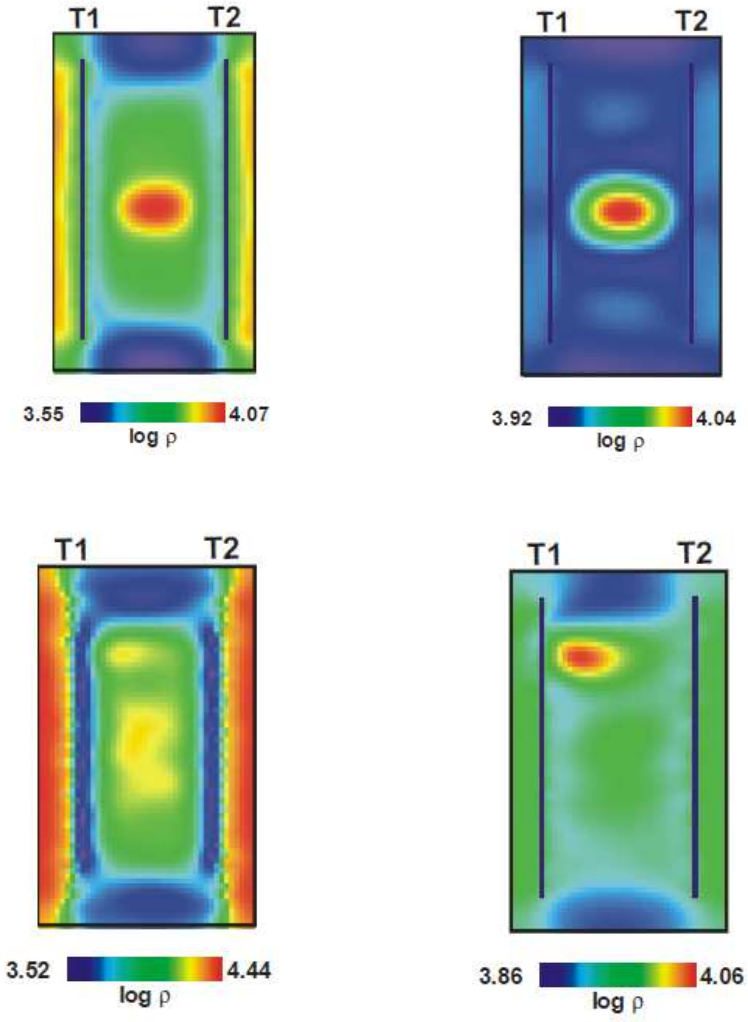

FIGURE 12
Inversion results for the 3D models depicted in Figure 10. In each case the first image represents the uncorrected results, while the second image shows the result following a difference-based correction applied to account for the interfering effect of layering in the background.

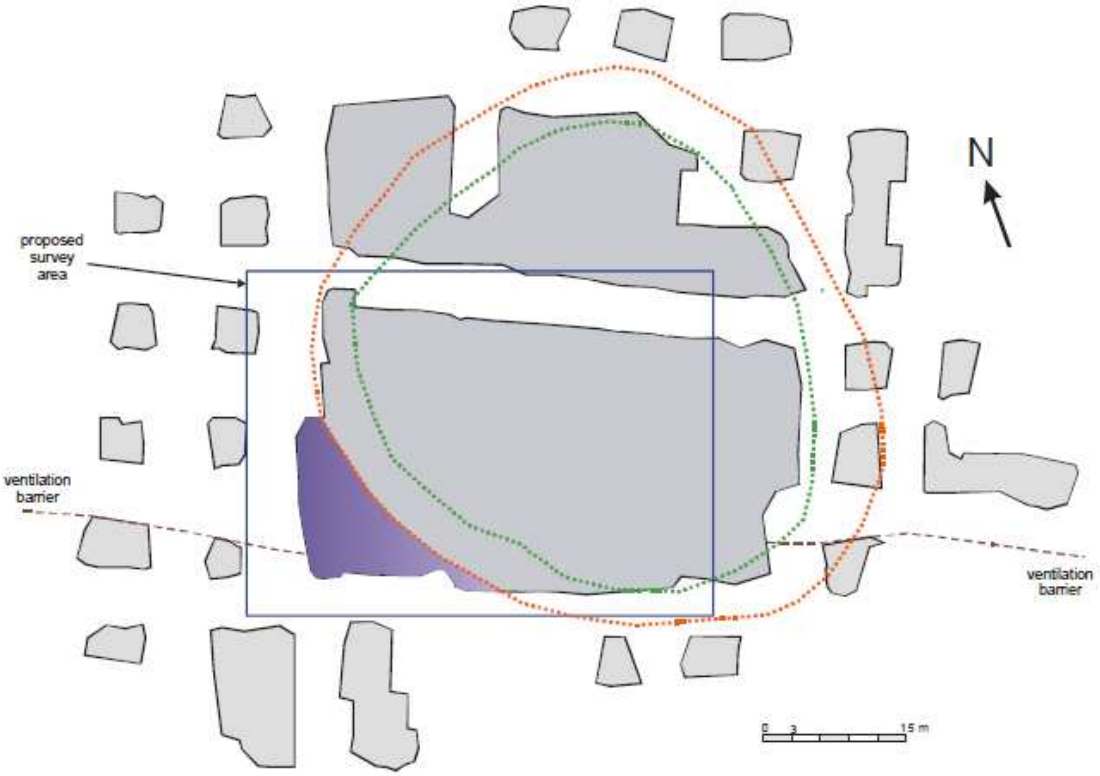

FIGURE 13
Schematic of ERT survey area at Waterval Mine. The darker shaded south-western corner of the large pillar represents a zone of UG2 reef that is not affected by the pothole, while the rest of the pillar effectively lies within the pothole structure. The orange dotted line indicates where the UG2 reef starts slumping, while the green dotted line indicates where the reef slumps into the footwall, below the floor of the developments.

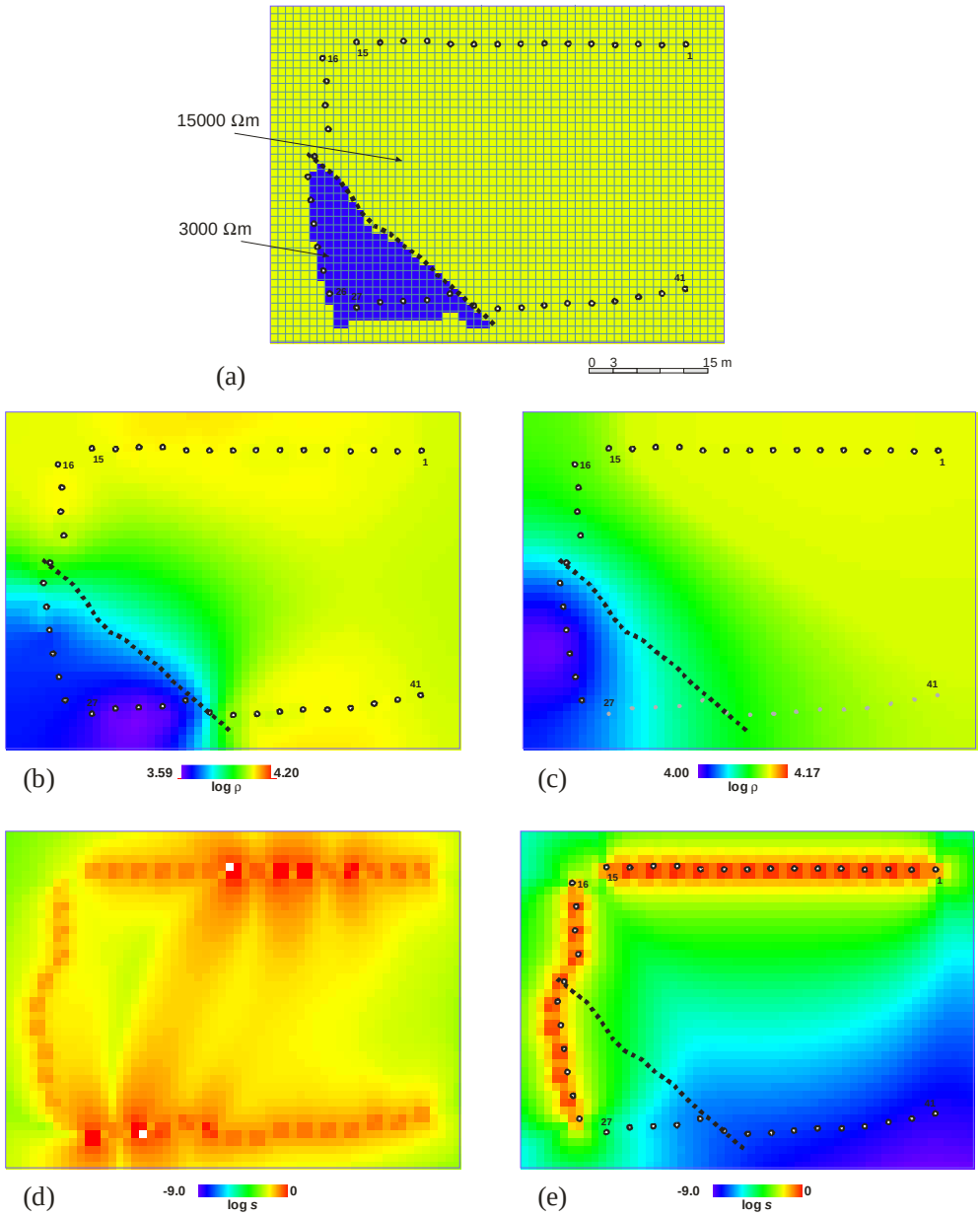

FIGURE 14
Waterval Mine ERT simulation model (a) and modelling results (b and c). Normalised accumulated sensitivity maps for the scenarios in (b) and (c) are shown in (d) and (e), respectively. These simulations highlight the difference in imaging performance when exploiting a total of 41 electrodes as was originally planned versus using only 26 electrodes as in the actual mine survey.

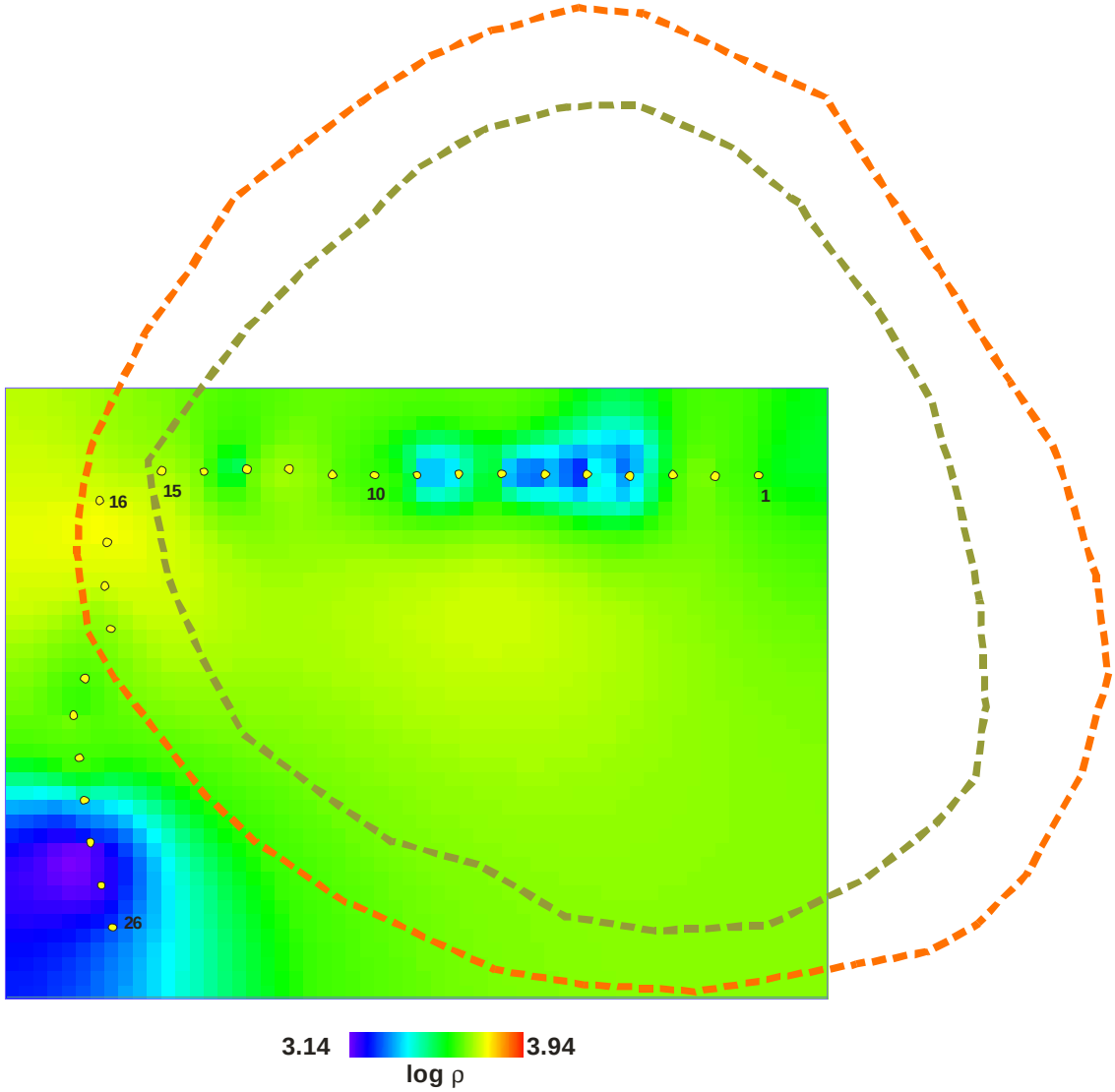

FIGURE 15
Waterval Mine ERT field data inversion result.